Metric Characteristics of Nuclear Rings and Related Features in Spiral Galaxies

R. Buta – University of Alabama
D. A. Crocker – University of Alabama

Citation of published version:

Buta, R., Crocker, D. (1993): Metric Characteristics of Nuclear Rings and Related Features in Spiral Galaxies. *The Astronomical Journal*, 105(4). DOI: 10.1086/116514

THE ASTRONOMICAL JOURNAL VOLUME 105, NUMBER 4 APRIL 1993

METRIC CHARACTERISTICS OF NUCLEAR RINGS AND RELATED FEATURES IN SPIRAL GALAXIES

R. BUTA[1,2,3] AND D. A. CROCKER[1]

Department of Physics and Astronomy, University of Alabama, Tuscaloosa, Alabama 35487

(Received 1992 August 25; revised 1992 November 20)

ABSTRACT

The metric properties of nuclear rings, pseudorings, spirals, and bars are discussed in the context of resonance theory and are used to gauge the range of sizes for such features. We find that the nuclear rings and pseudorings of strongly barred galaxies (types SB and SA$\underline{B}$) have a wide range in linear diameter, from about 0.4 kpc in ESO 566−24 to 3.8 kpc in ESO 565−11. The mean diameter is about 1.1 kpc for a sample of 20 objects. We suggest that there are clear analogues of the nuclear rings of strongly barred spirals in both weakly barred (SAB and S$\underline{A}$B) and nonbarred (SA) spirals. The size ratios of nuclear rings with respect to outer rings and pseudorings, as well as morphological characteristics, are best explained if outer rings and pseudorings are linked to the outer Lindblad resonance, and nuclear rings, pseudorings, and spirals are linked to the inner Lindblad resonance. These resonance identifications are consistent with most recent deductions. Nuclear bars are often associated with nuclear rings and spirals, but also can exist independently of such features. We present a list of 13 double-barred galaxies and discuss the significance of the phase angle of the nuclear bar with respect to the primary bar.

1. INTRODUCTION

Nuclear rings are the small rings of young stars often found in the centers of early type barred and oval disk galaxies. A typical example, NGC 1343, is illustrated in Fig. 1. The best-known example is found in NGC 1097 (Sersic 1958; Burbidge & Burbidge 1960), while others are illustrated as "hot-spot" nuclei by Morgan (1958), Sandage (1961), and Sersic & Pastoriza (1965, 1967). The rings tend to be rich in gas as well as in young stars and dust, and serve as a focal point for understanding star-formation processes and dynamics in the near-nuclear regions of galaxies (e.g., Osmer *et al.* 1974; Schweizer 1980; Buta 1986b, 1990; Hummel *et al.* 1987; Arsenault *et al.* 1988; Gerin *et al.* 1988; Pogge 1989; Garcia-Barreto *et al.* 1991a,b; Benedict *et al.* 1992). The high surface brightness of the rings makes them amenable to kinematic observations, and the gas velocity fields of several have been mapped in detail (e.g., Rubin *et al.* 1975; Rubin 1980; Peterson & Huntley 1980; Lindblad & Jorsater 1981; Meaburn *et al.* 1981; Buta 1986b, 1988; Arsenault *et al.* 1988; Schommer *et al.* 1988; Devereux *et al.* 1992). The most detailed optical/infrared study of any nuclear ring has been made by Benedict *et al.* (1992) in the well-known case of NGC 4314. Several nuclear rings are illustrated in color by Wray (1988). A starburst nuclear ring was detected in NGC 7469 with 6 cm VLA observations by Wilson *et al.* (1991).

Nuclear rings are potentially powerful probes of internal dynamics. Most authors seem to agree that nuclear rings are related to an inner Lindblad resonance, or ILR, based on model expectations (e.g., Simkin *et al.* 1980; Combes & Gerin 1985). This is probably the most reasonable interpretation, not only because of the properties of periodic orbits near the ILR (e.g., Contopoulos & Grosbol 1989), but also because of the ability of the bar to transport large amounts of gas to the central region (e.g., Kormendy 1982). An additional effect expected when an ILR is present is the enhancement of shocks and leading dust lanes in bars (e.g., Roberts *et al.* 1979; Athanassoula 1992). It is believed that growth of giant molecular clouds would be very effective at an ILR (Combes & Gerin 1985), and that this can explain the enhanced star-formation rates and, possibly, also the infrared excess detected from the SB galaxies containing nuclear rings (Hawarden *et al.* 1986).

Our interest in nuclear rings was considerably enhanced by the discovery of a spectacular example in the southern peculiar barred galaxy ESO 565−11 (Buta & Crocker 1991, hereafter referred to as BC). CCD images, shown in Fig. 11 of BC, reveal a large ring of bright blue associations in the center of the bar. The galaxy was observed as part of an imaging survey of early type galaxies selected on the basis of the appearance of an outer ring or pseudoring. Of 29 galaxies in the BC survey, 14 were found to have nuclear star formation, 9 in the form of blue nuclear rings, and 5 in the form of simple blue nuclei. Although a few of these were already known from previous work, it was not possible to identify nuclear rings in these galaxies *a priori* since the sample was selected from the *Catalogue of Southern Ringed Galaxies* (CSRG, Buta 1991a), which is based on the SRC-J sky survey. The SRC films have a small

[1]Visiting Astronomer, Cerro Tololo Inter-American Observatory, National Optical Astronomy Observatories, which is operated by the Association of Universities for Research in Astronomy, Inc. (AURA), under cooperative agreement with the National Science Foundation.
[2]Visiting Astronomer, Kitt Peak National Observatory, National Optical Astronomy Observatories, which is operated by AURA, under cooperative agreement with the National Science Foundation.
[3]Visiting Astronomer, Lowell Observatory.

 0004-6256/93/041344-14$00.90

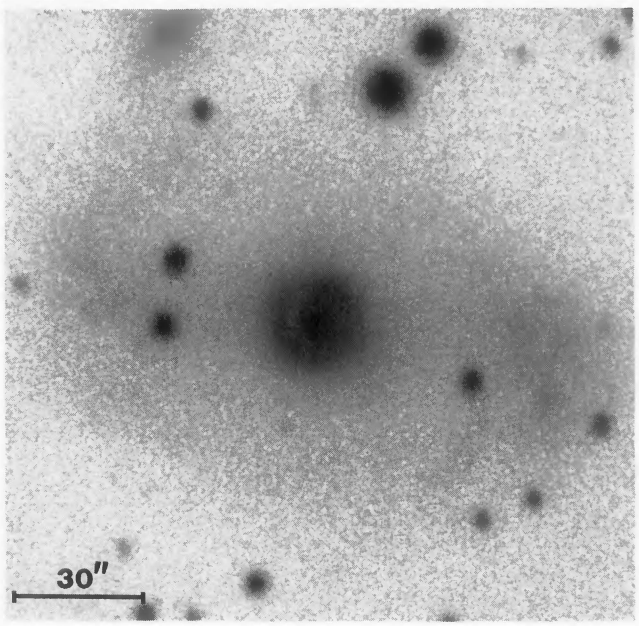

FIG. 1. *V*-band image of NGC 1343 and its bright nuclear ring obtained with the Lowell Observatory 1.1 m telescope and the NSF TI CCD. The image was taken under partly cloudy conditions and is not accurately calibrated. It is displayed in logarithmic units.

image scale and galaxy images are frequently overexposed in the cores. Thus, such image material is poorly suited to detecting nuclear rings. The multicolor CCD images in the BC survey were ideal for detecting nuclear rings because the typical blue colors make the rings prominent in color index maps, even when they are not obvious in direct blue-light images. The high rate of return of finding nuclear rings in outer-ringed galaxies has motivated us to carry out a detailed *IRAS* study of ringed galaxies (Crocker & Buta 1993).

In this paper, we present a systematic study of the metric properties of a relatively large sample of nuclear rings and related features. Our objective is to use the appearance of the rings, their surroundings, and their relative sizes with respect to other ring components to further evaluate the ILR hypothesis of their origin. The paper focuses on metric properties because these are the simplest characteristics to measure and they help to highlight some of the diversity in the phenomenon. In a separate paper we will discuss the photometric and color properties of nuclear rings.

2. COMPILATION OF NUCLEAR FEATURES

For our study we have compiled a list of as many examples of nuclear rings as we could find. We include in our study not only the best defined rings, but also features that have been called "nuclear pseudorings" and "nuclear spirals." These features are clearly related to nuclear rings and may represent a variation on the same phenomenon. In at least two galaxies that we know of, NGC 4314 (Benedict *et al.* 1992) and IC 4214 (BC), a nuclear ring and a nuclear spiral coexist. Some nuclear pseudorings or spirals could represent partly obscured nuclear rings or blue nuclei. In any case, the three types of features in a way define a "nuclear variety" similar to the "(r)," "(rs)," and "(s)" subclasses in the de Vaucouleurs revised Hubble system (de Vaucouleurs 1959).

Our sample consists of the 64 galaxies listed in Table 1, which gives the major and minor axis dimensions of nuclear rings and spirals. Since we are interested in estimating ring ratios, similar information is given for inner and outer rings or pseudorings should they be present in the same galaxy. The ring interpretations and dimensions are based on photographs from a variety of sources. For nuclear rings, these sources are given in the notes to Table 1. Almost all of the measurements were made by us. If we could make more than one measurement from different sources of photographs, or if a published source gave an estimate of the ring dimensions, then Table 1 gives an average of the available estimates. A useful source for identifying or verifying nuclear rings was the beautiful color atlas of Wray (1988). We used this atlas to measure nuclear ring dimensions for seven objects by determining the scale of the relevant images from local field stars as seen on the Palomar Sky Survey (hereafter referred to as PSS). Some care was necessary, however, in interpreting the images in this atlas. We have excluded about a dozen cases, typified by NGC 4596, where there is a smooth ringlike feature visible in the center of Wray's image that we believe could be a false ring caused by the image processing. These need verification with new images.

The most objective nuclear ring measurements are based on visual mapping of the rings from CCD images using a cursor on a television display. We were able to do this for 22 of the objects in Table 1 (source="CCD") from our own library of CCD images accumulated since 1990, both published (BC) and unpublished. The library includes *BVI* observations made with the CTIO 1.5 m telescope, the KPNO 0.9 m telescope, and the Lowell 1.1 m telescope during the period 1990 February–1992 August. Most of the unpublished images will be presented in later papers. Each galaxy was inspected for a nuclear ring, and if one was conspicuous in blue light, its shape parameters were based on the blue light image. However, if the ring was not a clear enhancement in blue light, but was most prominent in a color index map, this map was used instead to define the shape parameters. Once the (x,y) coordinates of the ridge line of the ring were determined, these coordinates were fitted with an ellipse to determine the dimensions. All other nuclear ring size estimates in Table 1 are based on visual measurements with a ruler or measuring magnifier.

Since many of the sample galaxies also have inner and outer rings or pseudorings, we collected all available measurements of the dimensions of those features. Such dimensions were available in de Vaucouleurs & Buta (1980), Kormendy (1979), Pedreros & Madore (1981), Buta (1984), Corwin *et al.* (1985, hereafter referred to as SGC), and the CSRG (phases I and II). Some of the inner and outer rings and pseudorings visible on our CCD images were also mapped and fitted with ellipses. For galaxies not recognized to have these features in the available sources, we examined them nevertheless on the PSS prints

TABLE 1. Apparent ring dimensions.

Name	D(O)	d(O)	n	O	D(I)	d(I)	n	I	D(N)	d(N)	n	N	Sources
NGC 210	4.10	2.20	1	R'_2	–	–	–	–	0.212	0.148	1	nrl	CCD
NGC 278	–	–	–	–	–	–	–	–	0.19	0.19	1	nr	P89
NGC 613	4.59	3.19	1	S	2.35	1.18	4	rs	0.240	0.198	1	ns	W88
NGC 986	3.38	2.49	4	R'_1	1.43	0.96	3	rs	0.310	0.161:	1	ns	W88
NGC 1068	5.19	4.48	2	R_1	–	–	–	–	0.50	0.35	1	nr′	V80
NGC 1097	6.80:	5.08	2	R'_1:	3.36	2.18	1	r′l	0.323	0.277	2	nr′	B84,H87
NGC 1300	5.71	4.92	1	R′	2.70	2.00	1	rs	0.150	0.110	2	nr	P89,CCD
NGC 1302	3.17	2.89	4	R	–	–	–	–	1.01	0.92	3	nr	V80,CSI,SGC
NGC 1317	3.26	2.91	3	R′	1.84	1.76	3	rl	0.432	0.335	2	nr	V80,S80
NGC 1326	2.61	1.78	3	R_1	1.07	0.85	3	r	0.196	0.148	1	nr	CCD
NGC 1343	–	–	–	–	1.75	1.29	1	r′l	0.277	0.257	2	nr	B84,CCD
NGC 1365	10.19	5.67	3	R′	–	–	–	–	0.818	0.387	1	ns	W88
NGC 1433	5.70	4.78	3	R'_1	2.89	2.14	3	r	0.300	0.233	2	nr	B84,B86b,(W88)
NGC 1512	5.50:	4.05:	2	S	2.40	1.85	3	r	0.280	0.221	1	nr′	B84,(W88)
NGC 1530	4.30	–	1	S	1.65	1.30	1	rs	0.400	0.224	1	ns	B84,(W88)
NGC 1543	5.29	4.82	5	R	2.63	2.15	3	l	0.371	0.353	1	nl	CCD
NGC 1808	6.36	4.13	3	R_1	3.34	1.52	1	l	0.226	0.164	1	nr′	CCD,(B84,W88)
NGC 1819	2.34:	1.85:	2	R_1?	1.12	0.76	1	l	0.105	0.078	1	nr	Dav92
NGC 2595	2.35	1.85	1	R′	1.06	0.85	1	rs	0.150	0.120	1	nr	W88
NGC 2681	2.25	2.09	2	R	–	–	–	–	0.57	0.57	1	nr	V80
NGC 2903	11.20	3.64	1	R'_1	2.50	1.40	1	rs	0.277	0.183	2	nr	B84,P89
NGC 2935	2.78	2.27	4	R'_2	0.85	0.60	1	l	0.106	0.094	1	nr	CCD
NGC 2997	7.33:	5.09:	1	S	–	–	–	–	0.16	0.086	1	nr	B84
NGC 3081	2.26	2.01	5	R_1	1.11	0.71	5	r	0.205	0.148	2	nr	B84,B90
NGC 3147	2.80	2.06	1	S	–	–	–	–	0.332	0.306	1	nr	W88
NGC 3313	3.30	2.79:	2	R'_1	1.43	1.08	3	r	0.144	0.139	1	nr	CCD
NGC 3351	5.49	3.57	2	R'_2	2.19	1.88	3	r	0.255	0.187	4	nr	R75,B84,P89,D92
NGC 3486	6.71	4.58	1	S	–	–	–	–	0.738	0.534	3	nr	S88,V80,PSS
NGC 3504	2.09	1.96	3	R'_1	1.07	0.69	1	r′l	0.148	0.095	1	nr	CCD
NGC 3593	–	–	–	–	–	–	–	–	0.340	0.153	1	nr	P89
NGC 4100	4.57	1.38	2	R′	3.20	0.90	1	r′l	0.195	0.088	1	nr	W88
NGC 4254	4.08	2.46	1	S	–	–	–	–	0.135	0.101	1	nr	P89
NGC 4303	5.50	5.09	2	S	1.67	1.59	2	rs	0.183	0.174	1	nr	P89
NGC 4314	3.62	2.76	2	R'_1	2.10	1.65	1	r′l	0.267	0.209	3	nr	B80,B84,P89
NGC 4321	4.96	3.77	2	S	2.01	1.40:	2	rs	0.347	0.233	3	nr′	B84,P86,P89
NGC 4526	–	–	–	–	–	–	–	–	0.497	0.271	1	nr	HA
NGC 4535	5.60	4.14	1	S	–	–	–	–	0.083	–	1	nr	B77
NGC 4826	6.00	2.55	1	R′	1.45	0.75	1	rs	0.198	0.157	1	nr	P89
NGC 4984	2.94	1.89	2	R	1.06	0.95	1	rl	0.218	0.170	1	nr	P89
NGC 5194	–	–	–	–	–	–	–	–	0.558	0.404	1	nr	W88
NGC 5236	9.29	8.95:	1	S	4.10	4.00	1	rs	0.15	0.135	1	nr	B84
NGC 5248	6.72	4.41	2	R'_1	2.40	1.10	1	rs	0.285	0.176	3	nr	B84,W88,P89
NGC 5383	5.10	3.53	2	R′	1.73	1.70:	1	rs	0.406	0.237	1	ns	W88
NGC 5427	1.96	1.57	1	S	–	–	–	–	0.257	0.184	1	nr	W88
NGC 5728	3.35:	2.48	2	R_1	1.82	0.90	3	r	0.144	0.127	2	nr	B84,CCD
NGC 5850	4.38	3.66	2	R′	2.10	1.68	4	r	0.258	0.216	2	nr	B84,CCD
NGC 5945	2.35	1.57	1	R_1	1.13	0.97	1	rs	0.124	0.105	1	nr	CCD
NGC 6753	1.89	1.64	4	R	1.11	0.89	4	rs	0.35	0.28	3	nr	B84
NGC 6782	1.96	1.51	4	R'_1	0.86	0.58	4	r	0.164	0.153	1	nr	CCD
NGC 6951	3.07	2.19	1	R'_1	1.47	1.04	2	rs	0.140	0.122	1	nr	W88
NGC 7217	2.50	2.10	1	R′	1.10	0.90	1	r′l	0.355	0.271	2	nr	V80,P89
NGC 7469	1.22	0.89	2	R	0.35	0.22	1	rs	0.062	0.050	1	nr	W91
NGC 7742	–	–	–	–	–	–	–	–	0.322	0.317	2	nr	V80,W88
IC 1438	2.04	1.91	2	R'_2	0.74	0.47	3	r	0.132	0.123	1	nr	CCD
IC 4214	1.97	1.22	4	R_1	0.91	0.48	4	rs	0.146	0.141	1	nr	CCD
UGC 12646	1.57	1.16	1	R'_1	0.70	0.45	1	r	0.084	0.065	1	nr	CCD
ESO 153–20	1.42	0.67	3	R'_1	0.63	0.58	3	rs	0.084	0.069	1	nr	CCD
ESO 198–13	2.23	1.68	3	R	0.79	0.60	3	r	0.246	0.205	1	nr	B86a
ESO 219–37	1.12	0.78	1	R′	–	–	–	–	0.216	0.168	3	nr	CSI,CSII,SGC
ESO 437–33	1.11	0.66	3	R'_1	0.39	0.26	1	rl	0.091	0.081	1	nr	CCD
ESO 437–67	2.48	1.96	2	R'_1	1.17	0.83	3	r	0.108	0.098	1	nr	CCD
ESO 507–16	0.90	0.68	2	R_1	0.40	0.24	3	rl	0.085	0.067	1	nr	CCD
ESO 565–11	2.52:	2.00	2	R′	1.28	1.01	3	rs	0.285	0.145	1	nr	CCD
ESO 566–24	1.17	0.58	1	R′	0.45	0.43	2	r	0.045	0.041	1	nr	CCD

Notes to TABLE 1

Col. 1: Object name
Cols. 2-3: Major and minor axis dimensions in arcminutes of outer feature (O)
Col. 4: Number of sources of outer feature measurements
Col. 5: Type of outer feature (R= outer ring; R′= outer pseudoring; R_1, R'_1= Type I Schwarz outer ring or pseudoring according to criteria of BC; R'_2= Type II Schwarz outer pseudoring according to criteria of BC; S = open outer spiral arms)
Cols. 6-7: Major and minor axis dimensions in arcminutes of inner feature (I)
Col. 8: Number of sources of inner feature measurements
Col. 9: Type of inner feature (r= inner ring; rs, rs, rs= inner pseudoring; l= inner lens; rl= inner ring/lens; r′l= inner pseudoring/lens)
Cols. 10-11: Major and minor axis dimensions in arcminutes of nuclear feature (N)
Col. 12: Number of sources of nuclear feature measurements
Col. 13: Type of nuclear feature (nr= nuclear ring; nr′= nuclear pseudoring; ns= nuclear spiral; nl= nuclear lens; nrl= nuclear ring/lens

TABLE 1. (continued)

Col. 14: Sources of dimensions for nuclear features only:
B77– Benedict et al. (1977)
B80– Benedict (1980)
B84– Buta (1984)
B86a– Buta (1986a)
B86b– Buta (1986b)
CCD– Measured from our CCD image or color index map
CSI– CSRG, phase I (Buta 1991)
CSII– CSRG, phase II
D92– Devereux et al. (1992)
Dav92– Davoust, 1992, private communication
HA– Hubble Atlas (Sandage 1961)
H87– Hummel et al. (1987)
P89– Pogge (1989)
PSS– Palomar Sky Survey
R75– Rubin et al. (1975)
S80– Schweizer (1980)
S88– Sandage and Bedke (1988)
SGC– Corwin et al. (1985)
W88– Wray (1988)
(W88)– Wray (1988), for confirmation only
W91– Wilson et al. (1991)
V80– de Vaucouleurs and Buta (1980)

or SRC/ESO surveys to see if such features may have gone unrecognized. This was the case for such well-known galaxies as NGC 1300, 2903, 3351, 5248, and especially 5383. For every case we at least tried to define an outer arm dimension, even if the arms do not clearly form an outer pseudoring. The outer feature classification in Table 1 includes the OLR subclasses R_1' and R_2' (BC), regular outer rings and pseudorings R and R′, and outer spiral arm dimensions S. The inner feature classifications include well-defined inner rings r, pseudorings $\underline{r}$s and rs, weak spiral pseudorings $\underline{r}$s, lenses l, and ring or pseudoring-lenses rl and r′l. Where possible, the measurements are based on averages if more than one estimate is available, but Table 1 does not give the specific sources of these measurements.

In some cases, the nuclear feature classification in Table 1 is less secure than the outer and inner feature classifications. We use the notation nr for closed nuclear rings, nr′ for nuclear pseudorings, and ns for nuclear spirals. The nuclear morphology comes from heterogeneous image material, and one can get a different impression from a different passband or different resolution image. For example, the data from Pogge (1989) are based on Hα images, where the rings might look very different from their blue-light appearance. Many of Pogge's galaxies are in the Wray (1988) atlas, and we checked the images there to see if the Hα feature could be detected. In cases like NGC 278, 1300, and 4254, we could not see a ringlike stellar component of the Hα ring in the Wray images. In the case of NGC 1300, Peterson & Huntley (1980) commented on the Hα nuclear ring as being visible in their spectra, and new CCD images recently added to our library show the ring clearly in blue light, thus confirming the existence of the feature. In some cases the nuclear feature is a very spotty hot-spot nucleus (Morgan 1958), and is not well defined as a ring. The complex feature in NGC 1808 is of this category but on our new *I*-band CCD image, we believe the feature is best characterized as a nuclear pseudoring. We have also reclassified the nuclear feature in NGC 1433 compared to Buta (1986b), whose 4 m CTIO prime focus plates suggested the classification nl (for nuclear lens). Our new *BVI* images obtained in very good seeing show a nuclear ring instead, emphasizing the importance of resolution.

Most of the nuclear features in Table 1 are sites of enhanced star formation, some more so than others. Some are certainly of the "starburst" variety, such as the nuclear pseudoring in NGC 1097 (Hummel *et al.* 1987). A couple of exceptions are NGC 5850 and ESO 153−20. The nuclear ring in NGC 5850 is not prominent in a $B-I$ color index map, while the nuclear ring in ESO 153−20 is clearly redder than its surroundings and may be more a ring of dust than of stars. In the center of NGC 1543, our new *BVI* images reveal a trace of a nuclear lens that is as red as the primary bar. It is clear that the color properties of nuclear rings and related features have a great deal of variety that must be explained.

Table 1 also includes speculative examples of nuclear rings in nonbarred or weakly barred galaxies. Almost all of these features have been or would be classified as *inner rings* in catalogues, yet the appearance suggests that they are very different from the conventional inner rings of SB galaxies. The subset includes NGC 1068, 1302, 2681, 3147, 3486, 4526, 4826, 5427, 6753, 7217, and possibly 7742. The list could be easily extended, and may include cases like NGC 4736 (Buta 1984) and the peculiar NGC 3310. In some of these cases there is an outer ring or pseudoring but no clear analogue of the inner rings in SB galaxies. Instead, there is an oval zone between the outer ring and the suspected nuclear ring that may act as the "bar" in some of these galaxies. NGC 2681 (Sandage 1961) is a particularly good example. NGC 1068 is similar in having a weak oval disk outside the nuclear pseudoring (Telesco & Decher 1988). These characteristics strongly suggest that the classified inner rings are really of the nuclear type. Also interesting in the nonbarred category is NGC 7217, which appears to be one of the most axisymmetric galaxies in the sample, and the very remarkable but uncertain case of NGC 7742, whose very bright ring is completely overexposed on the PSS but beautifully illustrated in Wray (1988). This latter object has no other rings and is worthy of further study.

3. METRIC PROPERTIES

3.1 Linear Diameters

To obtain linear nuclear ring diameters, we used the radial velocity as a distance indicator in most cases. The radial velocities were taken from RC3 (de Vaucouleurs *et al.* 1991), taking weighted averages of optical and radio radial velocities where available, and were reduced to what de Vaucouleurs & Peters (1981) and de Vaucouleurs *et al.* (1981) call the frame of reference defined by nearby galaxies, based on a solar motion solution with short scale distances. The apex of this motion, $l=120°$, $b=+28°$, and its amplitude, 320 km s^{-1}, were used in conjunction with a Hubble constant of 100 km s^{-1} Mpc^{-1} to get the distances. For the nearest galaxy in our sample, NGC 5236, the distance was taken from de Vaucouleurs (1979). For the Virgo Cluster galaxies NGC 4303, 4321, 4526, and 4535, we have adopted a distance of 13.9 Mpc from de Vaucouleurs (1982).

Table 2 summarizes the resulting linear diameters, D_l, in kpc, of the features in Table 1. The adopted distance, Δ, is given in Mpc, and where possible an estimate of the absolute blue magnitude is given using data from the RC3, Lauberts & Valentijn (1989), and Buta & Crocker (1992). The absolute magnitudes are in the range -18 to -21. Also given in Table 2 are the numerical Hubble type, T, from RC3 and an estimate of the "family" parameter, usually from RC3 but in some cases from our new CCD images where available. We divide the sample into groups SB and SA$\underline{\text{B}}$, SAB and S$\underline{\text{A}}$B, and SA.

The results show a wide range in diameters of nuclear rings. The smallest, in NGC 5236, is only $\approx$0.2 kpc in diameter, while the largest, in NGC 1302, is 4.6 kpc in diameter (if this feature is truly a nuclear ring). Among the true SB cases, the nr in ESO 565$-$11 stands out as an exceptional example. The object is listed in Table 2-1 of Buta (1984) as MCG $-3-24-12$, and was noted by Corwin (1983, private communication to Buta) to have a nuclear ring on a PSS copy plate. The object was rediscovered by Buta during the production of the CSRG, but the extreme nature of the nuclear ring became clear only after the radial velocity of the galaxy was measured. A preliminary reduction of 2D-Frutti observations with the CTIO 1.0 m telescope (Crocker 1993, in preparation) gave $V_\odot = 4662$ km s^{-1}. The nuclear ring of ESO 565$-$11 has an angular diameter comparable to some of the best known cases, such as in NGC 1097, 1433, 1512, and 4314, yet the galaxy is 3–5 times as distant. The linear diameter comes out to be 3.8 kpc, more than 2σ larger than the mean. The morphology of the bar and outer structures of the galaxy are peculiar; in fact, we believe that ESO 565$-$11 is a possible example of a galaxy where the inner ring and the bar are intrinsically misaligned (Crocker *et al.* 1993). We have obtained new imaging Fabry–Perot interferometry of this object that has confirmed the high radial velocity and that should shed much-needed light on its internal dynamics; this will be discussed in a separate paper.

Another interesting case is NGC 1343, whose nuclear ring is also visible on the PSS. In this case, detectability on the PSS is favored by a high foreground galactic extinction, which prevented the ring from being overexposed. Figure 1 displays a recently obtained CCD image, and shows that the galaxy includes a weak bar and inner ring lens which is very elongated. No outer ring or pseudoring is detectable on the PSS, though a very deep large format CCD image might reveal one. Our image was obtained with a TI CCD on the Lowell 1.1 m telescope and does not have the field of view to reveal a faint outer ring, if present. The nuclear ring is 2 kpc in diameter, and again is one of the largest among the clear-cut cases.

The CSRG includes other promising cases of nuclear rings which will be imaged later. Several of these are included in Tables 1 and 2. The nuclear ring in ESO 198$-$13 was noticed on an ESO-B copy film and is illustrated in Buta (1986a). The galaxy is a peculiar three-ring SA system having a RC3 radial velocity of 6200 km s^{-1}, and if the nr is real it would have an exceptional linear diameter, about 4 kpc. This is not surprising because we would expect that any clearcut nr visible on the sky survey charts in a rather faint, small galaxy would be larger than the average. Other candidate nr galaxies will be presented in Crocker & Buta (1993).

Figures 2(a)–2(c) display the log of the nuclear, inner, and outer ring, or pseudoring linear diameters vs Hubble stage for the SB and SA$\underline{\text{B}}$ subset, while Figs. 3(a)–3(c) display the same for the SA, S$\underline{\text{A}}$B, SAB subsets. The horizontal lines in *both* Figs. 2(a)–2(c) and 3(a)–3(c) are the means over the SB and SA$\underline{\text{B}}$ subset. These means are compiled in Table 3 and show that among strongly barred galaxies, nuclear, inner, and outer rings and pseudorings average about 1.1, 9.5, and 22.4 kpc in diameter, respectively. A significant fraction of the large standard deviation in the size of each of these features undoubtedly comes from the low quality of relative distances provided by redshifts. Note also that our sample is not volume limited.

The five nuclear spirals in our strongly barred sample average quite a bit larger than the nuclear rings: $\langle \log D_l \rangle = 0.34 \pm 0.10$ ($\sigma_1 = 0.25$); this gives about twice the average nuclear ring and pseudoring diameter, but the sample is too small to judge its significance. The nuclear spiral in NGC 1365 has been studied kinematically by Teuben *et al.* (1986), who deduce that it extends to near an ILR. This is also clearly indicated in the model of another barred galaxy with a nuclear spiral, NGC 5383, by Duval & Athanassoula (1983).

Since the horizontal lines in Fig. 3 are the same as in Fig. 2, we are able to judge the metric characteristics of rings in nonbarred and weakly barred galaxies in direct comparison to strongly barred ones. The results show that the definite and suspected nuclear rings in such galaxies scatter about a similar mean as for SB and SA$\underline{\text{B}}$ galaxies, but the inner and outer rings and pseudorings are smaller on average. The scatter in nuclear feature dimensions also seems larger than for the strongly barred cases, and there is hint of a weak type dependence in the sense that nuclear features in late-type spirals are smaller on average than those in earlier Hubble types.

TABLE 2. Linear diameters and feature ratios.

Name	F	T	M_T^o	Δ	D_ℓ(O)	D_ℓ(I)	D_ℓ(N)	$\frac{D(O)}{D(N)}$	$\frac{D(O)}{D(I)}$	$\frac{D(I)}{D(N)}$
NGC 613	SB	4.0	−20.1	13.1	17.5	9.0	0.9	19.1	2.0	9.8
NGC 986	SB	2.0	−19.8	18.0	17.6	7.5	1.6	10.9	2.4	4.6
NGC 1097	SB	3.0	−20.3	11.0	21.8	10.8	1.0	21.1	2.0	10.4
NGC 1300	SB	4.0	−20.0	14.5	24.1	11.4	0.6	38.1	2.1	18.0
NGC 1365	SB	3.0	−20.9	14.6	43.4	–	3.5	12.5	–	–
NGC 1433	SB	2.0	−18.9	8.2	13.7	6.9	0.7	19.0	2.0	9.6
NGC 1512	SB	1.0	−18.1	6.6	10.6	4.6	0.5	19.6	2.3	8.6
NGC 1530	SB	3.0	−20.8	27.7	34.6	13.3	3.2	10.8	2.6	4.1
NGC 1543	SB	−2.0	−18.2	8.2	12.6	6.2	0.9	14.3	2.0	7.1
NGC 1819	SB	−2.0	−20.6	44.8	30.5	14.6	1.4	22.3	2.1	10.7
NGC 2935	SAB	3.0	−19.8	21.5	17.4	5.3	0.7	26.2	3.3	8.0
NGC 3313	SB	2.4	−20.8	36.0	34.6	15.0	1.5	22.9	2.3	9.9
NGC 3351	SB	3.0	−19.4	8.4	13.4	5.3	0.6	21.5	2.5	8.6
NGC 3504	SAB	2.0	−19.6	16.9	10.2	5.2	0.7	14.1	2.0	7.2
NGC 4314	SB	1.0	−19.1	11.3	11.8	6.9	0.9	13.6	1.7	7.9
NGC 5383	SB	3.0	−20.0	24.7	36.6	12.4	2.9	12.6	2.9	4.3
NGC 5728	SAB	1.0	−20.4	27.1	26.4	14.3	1.1	23.3	1.8	12.6
NGC 5850	SB	3.0	−20.7	25.7	32.8	15.7	1.9	17.0	2.1	8.1
NGC 5945	SB	2.0	−20.3	57.5	39.3	18.9	2.1	19.0	2.1	9.1
NGC 6782	SAB	0.8	−20.6	36.2	20.7	9.1	1.7	12.0	2.3	5.2
UGC 12646	SB	3.0	−20.9	81.7	37.3	16.6	2.0	18.7	2.2	8.3
ESO 153−20	SB	2.6	−20.2	56.6	23.4	10.4	1.4	16.9	2.3	7.5
ESO 437−67	SB	2.1	−19.3	29.9	21.6	10.2	0.9	23.0	2.1	10.8
ESO 565−11	SB	0.3	−19.8	45.4	33.3	16.9	3.8	8.8	2.0	4.5
ESO 566−24	SB	3.7	−19.4	34.1	11.6	4.5	0.4	26.0	2.6	10.1
NGC 210	SAB	3.0	−19.6	15.5	18.5	–	1.0	19.3	–	–
NGC 278	SAB	3.0	−19.0	8.7	–	–	0.5	–	–	–
NGC 1302	SAB	0.0	−19.5	15.5	14.3	–	4.6	3.1	–	–
NGC 1317	SAB	1.0	−19.4	17.4	16.5	9.3	2.2	7.5	1.8	4.3
NGC 1326	SAB	−1.0	−18.9	11.6	8.8	3.6	0.7	13.3	2.4	5.5
NGC 1343	SAB	3.0	−20.2	25.1	–	12.8	2.0	–	–	6.3
NGC 1808	SAB	1.0	−19.1	8.0	14.8	7.8	0.5	28.1	1.9	14.8
NGC 2595	SAB	4.5	−20.6	44.4	30.3	13.7	1.9	15.7	2.2	7.1
NGC 2681	SAB	0.0	−19.0	9.3	6.1	–	1.5	3.9	–	–
NGC 2903	SAB	4.0	−20.0	6.7	21.7	4.8	0.5	40.4	4.5	9.0
NGC 2997	SAB	5.0	−20.5	9.2	19.5	–	0.4	45.8	–	–
NGC 3081	SAB	0.0	−19.2	22.4	14.7	7.2	1.3	11.0	2.0	5.4
NGC 3486	SAB	5.0	−18.8	8.3	16.3	–	1.8	9.1	–	–
NGC 4303	SAB	4.0	−20.6	13.9	22.2	6.7	0.7	30.1	3.3	9.1
NGC 4321	SAB	4.0	−20.7	13.9	20.1	8.1	1.4	14.3	2.5	5.8
NGC 4526	SAB	−2.0	−20.2	13.9	–	–	2.0	–	–	–
NGC 4535	SAB	5.0	−20.4	13.9	22.6	–	0.3	67.5	–	–
NGC 4984	SAB	−1.0	−18.2	11.3	9.7	3.5	0.7	13.5	2.8	4.9
NGC 5236	SAB	5.0	−19.9	3.7	10.0	4.4	0.2	61.9	2.3	27.3
NGC 5248	SAB	4.0	−19.8	12.1	23.7	8.5	1.0	23.6	2.8	8.4
NGC 6951	SAB	4.0	−20.5	17.2	15.4	7.4	0.7	21.9	2.1	10.5
NGC 7469	SAB	1.0	−20.8	49.5	17.6	5.0	0.9	19.7	3.5	5.6
IC 1438	SAB	0.7	−19.5	25.0	14.9	5.4	1.0	15.5	2.8	5.6
ESO 219−37	SAB	8.0	–	–	–	–	–	5.2	–	–
ESO 437−33	SAB	1.0	−19.3	33.2	10.7	3.8	0.9	12.2	2.8	4.3
ESO 507−16	SAB	0.4	−19.8	68.8	18.0	8.0	1.7	10.6	2.3	4.7
NGC 1068	SA	3.0	−20.8	11.2	17.0	–	1.6	10.4	–	–
NGC 3147	SA	4.0	−21.2	31.2	25.4	–	3.0	8.4	–	–
NGC 3593	SA	0.0	−17.8	7.0	–	–	0.7	–	–	–
NGC 4100	SA	4.0	−19.6	13.2	17.5	12.3	0.7	23.4	1.4	16.4
NGC 4254	SA	5.0	−20.6	13.9	16.5	–	0.5	30.2	–	–
NGC 4826	SA	2.0	−19.8	5.3	9.3	2.3	0.3	30.3	4.1	7.3
NGC 5194	SA	4.0	−20.6	7.0	–	–	1.1	–	–	–
NGC 5427	SA	5.0	−20.4	26.2	14.9	–	2.0	7.6	–	–
NGC 6753	SA	3.0	−20.7	28.8	15.8	9.3	2.9	5.4	1.7	3.2
NGC 7217	SA	2.0	−19.7	11.2	8.1	3.6	1.2	7.0	2.3	3.1
NGC 7742	SA	3.0	−18.9	17.1	–	–	1.6	–	–	–
IC 4214	SA	1.5	−20.0	21.2	12.1	5.6	0.9	13.5	2.2	6.2
ESO 198−13	SA	2.1	−20.5	59.5	38.6	13.7	4.3	9.1	2.8	3.2

Notes to TABLE 2

Col. 1: Object name
Col. 2: RC3 family, or revised family from CCD images
Col. 3: RC3 numerical stage index
Col. 4: Absolute total blue magnitude (RC3 corrections)
Col. 5: Adopted distance (Mpc)
Cols. 6–8: Linear major axis feature diameters in kpc
Col. 9–11: Feature apparent diameter ratios

3.2 Ring Ratios

We now consider the ratios of the sizes of rings within the same galaxy. These are important distance-independent quantities that can be tied directly to theory. We have pointed out that the most promising interpretation of nuclear rings is that they lie near an ILR of a bar or oval. There are no direct ways of evaluating this idea without a detailed dynamical model and kinematic data. However, one of the simplest indirect methods is to use ratios of ring sizes in double-, or triple-ring systems. These systems are very common among early-to-intermediate Hubble-type barred spirals and S0s (see Table 1 of Buta 1991a). If nuclear, inner, and outer rings and pseudorings in normal galaxies are, in general, related to a few specific major

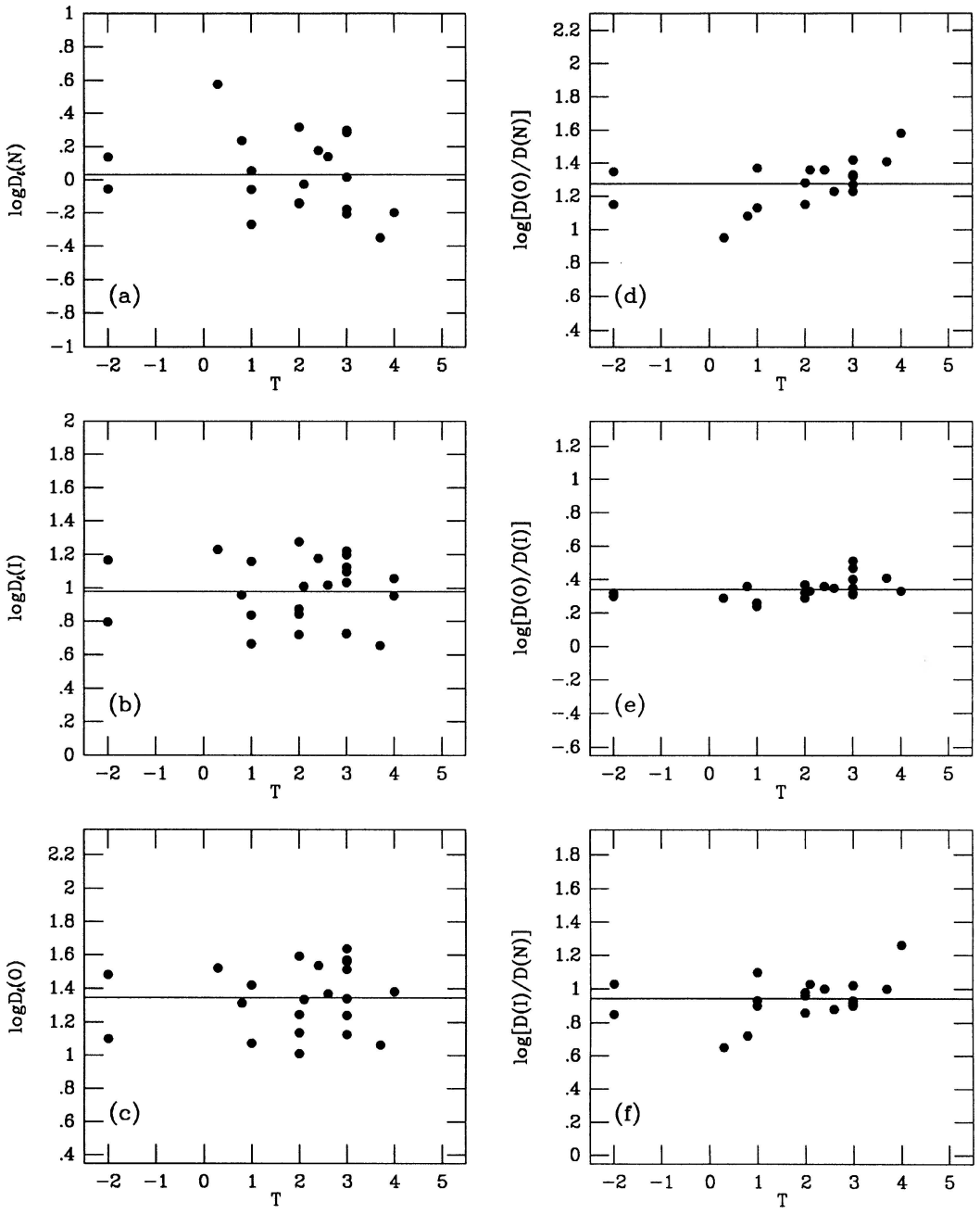

FIG. 2. Linear ring diameters D_l and apparent ring diameter ratios vs RC3 Hubble stage T for the strong-barred galaxy sample (those classified as being SB and SAB types in Table 2). The leftmost panels are (a) nuclear rings and pseudorings; (b) inner rings and pseudorings; and (c) outer rings and pseudorings. The rightmost panels are: (d) the outer to nuclear ring and pseudoring ratio; (e) the outer to inner ring and pseudoring ratio; and (f) the inner to nuclear ring and pseudoring ratio. The horizontal lines are the means over the samples. These plots exclude the ns and S features in Table 2.

resonances, then the ratios of the sizes of rings in double- or triple-ringed galaxies will reflect the properties of the rotation curve and the pattern speed (Athanassoula *et al.* 1982). The main resonances we are concerned with are the ILR, the OLR, and the inner 4:1 resonance, because these are the resonances which n-body models (Schwarz 1979; Combes & Gerin 1985) have suggested are linked to nuclear, outer, and inner rings, respectively. Table 4 provides a convenient cross index of features for reference. We also consider ratios with respect to the corotation resonance, CR.

Our sample includes galaxies where the *morphology* of an outer ring or pseudoring resembles model rings which have formed near the OLR in the n-body models of

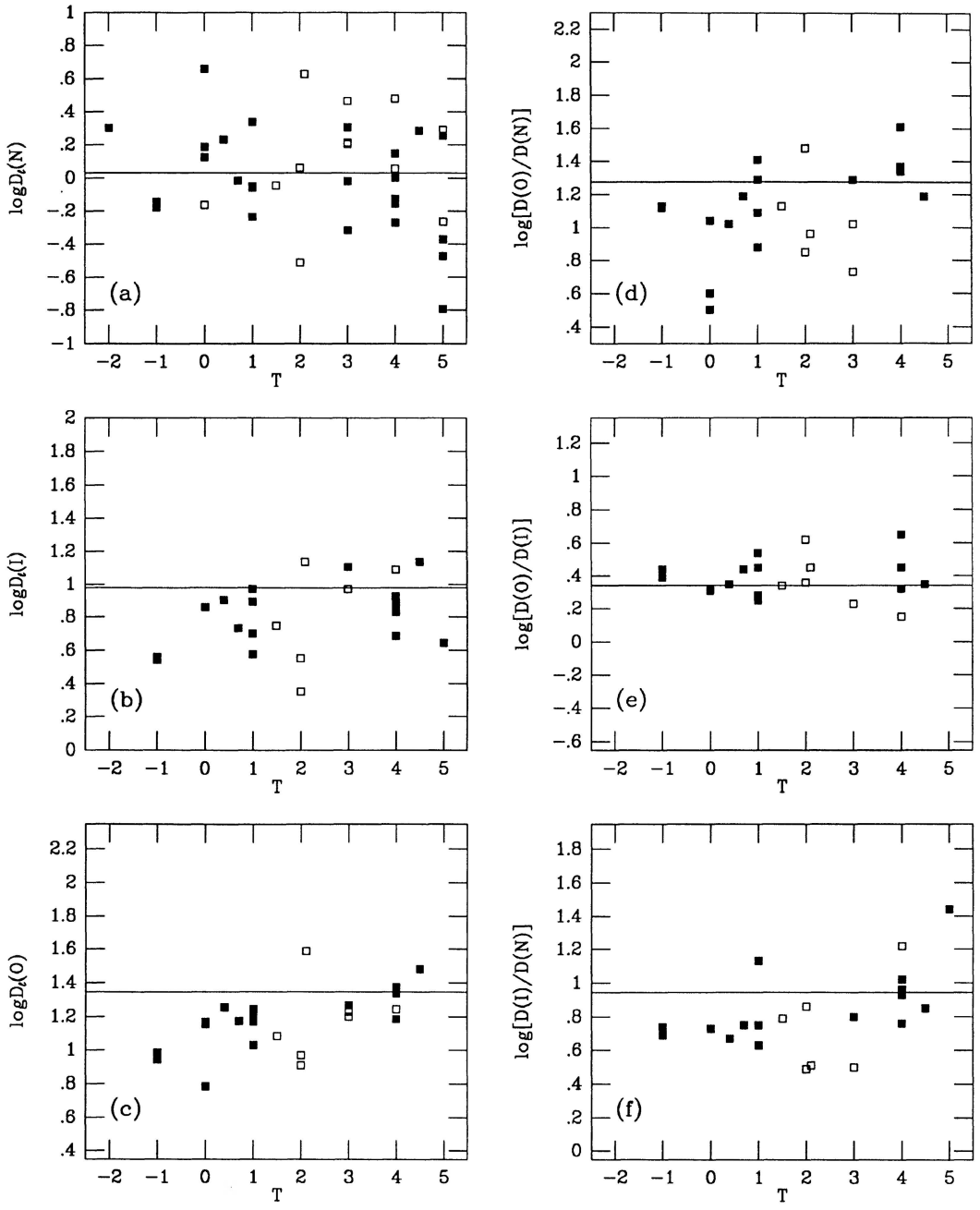

FIG. 3. Same panels as in Fig. 2, for the SA (open squares), and SAB, SAB (filled squares) samples. The horizontal lines are the same as in Fig. 2.

Schwarz (1981). These are designated with the notation R_1, R_1', and R_2' (see Fig. 1 of BC). Any galaxy in our sample displaying one of these morphologies is so indicated in column 5 of Table 1. The identification of these OLR morphologies in real galaxies makes the ring ratio method more powerful than it might otherwise be because one ring feature can be uniquely identified. For our analysis we will assume that any outer ring or pseudoring feature in Table 1 is an OLR feature, even if it is not classified in the BC OLR subcategories. The last three columns of Table 2 give values of the outer to nuclear feature ratio, $D(O)/D(N)$, the outer to inner feature ratio, $D(O)/D(I)$, and the inner to nuclear feature ratio, $D(I)/D(N)$. The logarithms of these ratios are plotted against RC3 type, T, in Figs. 2(d)–2(f) and 3(d)–3(f). For the strongly barred sample, the means of the logarithmic ratios are compiled in Table 3,

TABLE 3. Mean logarithmic diameters D_l(kpc) and diameter ratios for SAB and SB galaxies.[a]

Parameter	Mean	σ_1	N
$\log D_\ell(O)$	1.345	0.196	22
$\log D_\ell(I)$	0.979	0.197	24
$\log D_\ell(N)$	0.031	0.237	20
$\log \frac{D(O)}{D(N)}$	1.276	0.143	19
$\log \frac{D(O)}{D(I)}$	0.342	0.065	21
$\log \frac{D(I)}{D(N)}$	0.942	0.128	20

Notes to TABLE 3

[a] Type range S0° to Sbc; excluding nuclear spirals and "S" features in Table 1

and are illustrated by the solid horizontal lines in Figs. 2(d)–2(f). For reference, these same horizontal lines are also plotted in Figs. 3(d)–3(f).

The results show first that the ratios have significantly less scatter than the linear diameters, particularly $D(O)/D(I)$. For the two ratios involving nuclear features, however, the standard deviation is more than twice that for $\log[D(O)/D(I)]$. The ranges of the ratios are $8.8 \leqslant D(O)/D(N) \leqslant 38.1$, $4.5 \leqslant D(I)/D(N) \leqslant 18.0$, and $1.7 \leqslant D(O)/D(I) \leqslant 3.3$, excluding the nuclear spirals. The logarithmic means in Table 3 imply average values of 18.9, 8.7, and 2.2 for $D(O)/D(N)$, $D(I)/D(N)$, and $D(O)/D(I)$, respectively. These results can be explained with the resonance identifications in Table 4 if the rotation curves of the sample galaxies rise gradually to maximum with different rates of rise and if there is a spread in pattern speeds. To illustrate this, we use a simple analytic expression that represents the appearance of many rotation curves (Elmegreen & Elmegreen 1990):

$$V(r) = \frac{r}{r^A + r^{1-\alpha}}, \qquad (1)$$

where A determines the rate of rise to maximum and α determines the flatness of the rotation curve at large radii. Figure 4(a) shows a few rotation curves for different values of A, while Figs. 4(b)–4(f) show how various resonance diameter ratios depend on A and the corotation radius, r(CR), for the case $\alpha = 0$ ($V \approx$ constant at large radii). The ILR diameter that we consider is that of the outermost inner Lindblad resonance, since rotation curves with low values of A have two ILRs. For A close to 0, all ratios with D(ILR) strongly depend on the radius of CR. The curves in Fig. 4(b) show that we can easily explain ratios $D(O)/D(N)$ of 9 to 38 by differences in the shapes of the inner parts of rotation curves and pattern speed differences. In contrast, the ratios D(OLR)/D(4:1) [Fig. 4(c)] and D(OLR)/D(CR) [Fig. 4(d)] are very insensitive to the differences between most rotation curves. These resonance identifications provide a reasonable explanation of why the scatter in the ratio $D(O)/D(I)$ is so much lower than for $D(O)/D(N)$ and $D(I)/D(N)$. The outer and inner features must be located, in general, on parts of the rotation curves which are less sensitive to bulge mass and central density than nuclear features. This may also explain the relative constancy of $D(O)/D(I)$ with Hubble type. However, if we assume that most rotation curves have $A < 0.6$, in order to account for the large spread in $D(O)/D(N)$, then the observed mean ratio $D(O)/D(I) = 2.2$ is not readily explained by the ratios D(OLR)/D(4:1) or D(OLR)/D(CR), at least within the limitations of the analytic rotation curve representation we have used; instead, the observed ratio is bracketed by the theoretical ones. Note that we have ignored the intrinsic shapes of the ring features for the observed ratios, but it is unlikely that rings are, in general, intrinsically circular (Buta 1986a). Since there is always a low probability of viewing an intrinsically oval ring exactly end on, noncircular intrinsic shapes could affect the ratios and make $D(O)/D(I)$ smaller than it should be (since we have used the apparent major axis dimension, not some kind of mean diameter). Note also that Eq. (1) does not allow for all of the possible bumps and wiggles that real rotation curves can display. For example, the rotation curve of NGC 6300 shows two levels of rotation caused by the self-gravity of a large spiral inner pseudoring (Buta 1987). Such a rotation curve therefore has an extra component that would affect the shapes of the Lindblad precession frequency curves.

The curves in Figs. 4(e) show that we expect the ratio $D(I)/D(N)$ to have a similar large scatter as the ratio $D(O)/D(N)$, for the resonance identifications in Table 4. This is certainly observed. We also expect a large spread in values for the ratio D(CR)/D(ILR), as shown in Fig. 4(f).

The ratios for the nonbarred and weakly barred samples in Table 2 show a much greater spread than the strongly barred sample ratios. Nevertheless, some of the nonbarred and weakly barred ratios are consistent with the strongly barred ratios, in particular for NGCs 1068, 1326, 1808, 2595, 3081, 4984, 5248, 6951, IC 1438, IC 4214, and ESOs 198−13, 437−33, and 507−16. Probably the same resonances are involved as for the strongly barred cases. However, the very large ratios, $D(O)/D(N) > 40$, for some of the late types such as NGCs 2903, 2997, 4535, and 5236, may require other interpretation, for example involving an inner ILR. In addition, four galaxies in Table 2, NGC 1302, 2681, 6753, and ESO 219−37, have ring ratios less than 5.8, the value of D(OLR)/D(ILR) expected for a pure V=constant rotation curve [obtained for $A = 1$ in Eq. (1)]. In these cases, the resonance identifications of the rings in Table 4 are doubtful. To explain these ratios with the OLR and ILR would require that the rotation curves be peaked with a significant drop off outside the peak. In Eq. (1), such rotation curves occur either for $A > 1$ (see Fig. 4(a)) or for $\alpha < 0$ (Elmegreen & Elmegreen 1990).

TABLE 4. Cross index of feature identifications.

	Outer feature	Inner feature	Nuclear feature
Tables	O	I	N
Classification	R,R′ R_1,R_1',R_2'	r,rs,rs,rs rl,r′l,l	nr,nr′,ns nrl,nl
Resonance	OLR	4:1	ILR

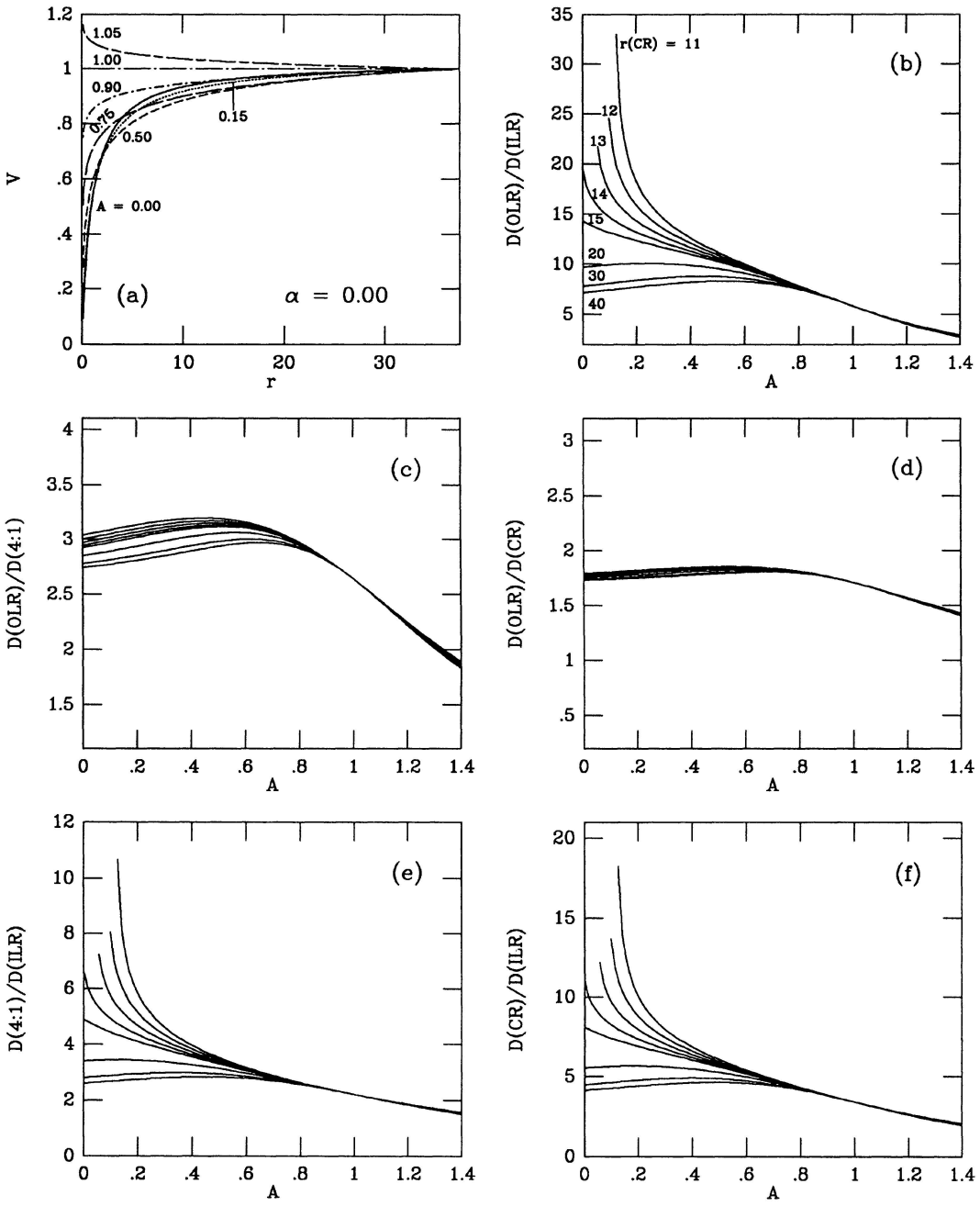

FIG. 4. Rotation curves and ring ratios for the simple representation $V(r)=r/(r^A+r^{1-\alpha})$ suggested by Elmegreen & Elmegreen (1990). The panels are (a) a few rotation curves for different values of A and $\alpha=0$, the latter ensuring that the curves are flat at large radii; each curve is normalized to unity at $r=40$; (b) the dependence on A of the ratio of the diameter of the OLR to the diameter of the ILR, for different values of the corotation radius r(CR); (c) same as (b) for the ratio of the diameter of OLR to that of the inner 4:1 resonance; (d) same as (b) for the ratio of the diameter of OLR to that of CR; (e) same as (b) for the ratio of the diameter of the inner 4:1 resonance and that of ILR; and (f) same as (b) for the ratio of the diameter of CR to that of ILR. The different curves in (c)–(f) are for the same corotation values as in (b), and are in the same order as the curves are labeled in (b). The different curves overlap almost completely in (d).

In summary, the resonance identifications in Table 4 provide a reasonable explanation of the observed ring ratios in strongly barred galaxies and in some weakly barred galaxies. When used in conjunction with other morphological evidence supporting the resonance interpretations for inner and outer rings and pseudorings (see, e.g., Buta 1986a,b, and BC), the identification of nuclear rings and pseudorings with an ILR seems very likely.

3.3 Intrinsic Shapes and Orientations

The problem of the intrinsic shapes of nuclear rings and their orientations with respect to bars can be addressed in

two ways. One approach is to obtain distributions of apparent axis ratios and relative bar/ring position angles for a large sample of nuclear rings and, under the assumption of extreme thinness and random spin orientations, deduce what intrinsic shapes and orientations can reproduce the observed distributions. Such an approach is unfeasible, however, for the following reasons: First, we have a list of only 64 cases of nuclear rings. Selection effects are important, and a much larger sample would be needed to say anything definitive. Second, the rings are not easy to define in some cases, so that shapes and orientations have a fair degree of uncertainty. Third, our list is inhomogeneous, and any homogeneous subsets we might choose from it will be even less useful for statistics.

Another, more useful, approach is to try and make deductions about nuclear rings from the appearance of the outer and inner ring features, or from galaxies known to have low inclinations from the shapes of faint outer isophotes. For example, if the outer feature is nearly circular in projection, we may deduce a low inclination, so that projection effects on the shape and orientation of the nuclear ring would be minimal. If we select only the objects in Table 1 which have an outer feature axis ratio of $b/a \geqslant 0.85$ (corresponding roughly to an inclination $< 35°$, if these features are intrinsically circular), we get the following eleven objects: NGCs 1068, 1300, 1302, 1317, 2681, 3081, 3504, 4303, 5236, 6753, and IC 1438. Of these, the best nuclear ring is found in NGC 1317, an object whose morphology has been extensively illustrated by Schweizer (1980) and whose nuclear ring is actually distinguishable on the ESO-B sky survey. Schweizer's Fig. 4 shows that a small bar lies inside the nr and greatly *underfills* it. The nr is elongated parallel to the nuclear bar, and both features are nearly perpendicular to a "fat" outer bar that must be the primary bar of the system. Since the galaxy appears virtually face on from the shapes of both its inner and outer features, then we have an example of a nuclear ring with a significant intrinsic elongation (axis ratio 0.78) and an intrinsic alignment of 90° with respect to a primary bar. Another very good nuclear ring, that in NGC 3081, is also likely to be intrinsically elongated at a large angle to a primary bar. Using the shape of the outer ring as an indication of inclination, Buta (1990) derived an intrinsic axis ratio of 0.82 for the nuclear ring, and a relative bar/ring position angle of 49°.

Of the remaining nine objects, the possible nuclear rings in NGC 1302 and 2681, as well as the definite nuclear ring in IC 1438, appear as round or rounder than the outer features, and thus must be nearly round intrinsically. The nuclear ring in NGC 3504 is only distinguishable clearly on the $B-I$ color index map of BC and its apparent axis ratio, 0.64, appears strongly affected by dust.

Among galaxies of known inclination, the two cases of NGC 1433 and 4314 are important for the shape and orientation problem. NGC 1433, studied by Buta (1986b), has an inclination in the range 20°–33° and a nuclear ring of intrinsic axis ratio ≈ 0.85 and bar/ring position angle $\approx 50°$, parameters very similar to NGC 3081. It demonstrates that intermediate alignments between nuclear rings and bars are observed. For NGC 4314, Benedict *et al.* (1992) used faint outer isophotes to deduce an inclination of only 23°. This object includes not only a nuclear ring but also a nuclear spiral which breaks from the major axis of the ring and winds into an oval at nearly a perpendicular angle. In this case the nuclear ring is virtually aligned with the bar, so the nuclear spiral is also perpendicular to the bar. The axis ratio of the nuclear ring in Table 1 is 0.78 and that of the nuclear spiral about 0.7 in Buta (1984).

Finally, we have obtained CCD images of NGC 3313, a nearly face-on strongly barred spiral which displays a very bright, virtually circular nuclear ring. These images will be presented in a later paper, but here we simply note that the galaxy has a very complex outer arm pattern, and the shape of the outer disk suggests that the inclination is no more than 35°. The nuclear ring could be an intrinsically circular example. However, no 21 cm line width is given for the galaxy in RC3 that might help us to gauge the inclination better.

We conclude from this analysis that nuclear rings have a range of intrinsic axis ratios and bar/ring alignments. Some may be intrinsically round, others oval or noncircular, and alignments can be parallel, perpendicular, or at intermediate angles. The fact that nuclear rings can be found at intermediate or perpendicular angles provides strong support for their interpretation in terms of ILR. An *n*-body model illustrated by Simkin *et al.* (1980) shows that in a simple barred galaxy model where a single ILR exists, a nuclear oval of gas obliquely aligned with a bar can develop, which over time aligns more and more perpendicularly to the bar. Misalignment is *not* predicted for inner and outer rings and pseudorings in such models, which is consistent with the observed alignment properties of most such rings (Buta 1986a). However, as will be discussed by Crocker *et al.* (1993), a small number of inner and outer rings may be characterized by intrinsic misalignment with respect to bars.

3.4 Presence of Dust Lanes

One characteristic of galaxies that seems to correlate with the presence of nuclear rings is the presence of dust lanes in the bar or oval. This was clear from some of the earliest known examples, such as NGC 1097 and 4314. Of the 29 BC galaxies, the 9 with a clear nuclear ring show a dust lane pattern in the region of a bar or oval. Most of these patterns are the normal, nearly straight leading dust lanes almost universally thought to be shocks (see, e.g., Roberts *et al.* 1979). Athanassoula (1992) has discussed how the appearance and existence of bar dust lanes in a galaxy depend on the shape of the bar and the existence of an ILR. It appears that an ILR is necessary but not sufficient to explain the leading dust lanes prominent in many SB galaxies. In weaker bars, these lanes are predicted to be more curved and irregular. Most of the galaxies in BC which lack an nr or blue nucleus show no evidence for dust within the bar or oval region, even when the bar seems

strong and significant. Thus, the presence of dust lanes supports the interpretation that the nuclear rings are related to ILR.

There are some exceptions. For example, ESO 565−11 does not have very strong dust lanes in the $B-I$ color index map in BC. There are also some regular but unusual patterns seen that merit further study. For example, Benedict *et al.* (1992) have found that the dust lanes in the bar of NGC 4314 curve around only half-way out along the bar length, causing them to speculate that the bar of this galaxy extends well beyond corotation, an unexpected result. In NGC 1326, BC found a more complex pattern of curved dust lanes which no model has predicted. These objects show that more theoretical work is needed.

3.5 Nuclear Bars

A few of the galaxies in Table 1 have a small bar *inside* the nuclear feature. Among the strongly barred cases, such a "nuclear bar" is prominent in our new CCD images of NGC 5850, and we have already pointed out the case of NGC 1317 as illustrated by Schweizer (1980). We have attempted to identify which other galaxies in Table 1 have such central bars. The Wray (1988) atlas shows that the nuclear spirals of NGC 613, 986, 1365, and 5383 could have associated nuclear bars, but the effects of dust are uncertain. Identification of nuclear bars is best made from near-infrared images, such as 2.2 μm images or I-band CCD images. Those in NGC 1068 (Scoville *et al.* 1988), NGC 1433 (Buta 1986b), NGC 3081 (Buta 1990), NGC 4321 (Pierce 1986), and several others in our CCD library were found in this way. We cannot give a firm number as to what fraction of nuclear rings include these features. However, it is clear that the two phenomena can exist independently. For example, NGC 1291 (de Vaucouleurs 1975; Jarvis *et al.* 1988) and NGC 1543 (Jarvis *et al.* 1988) display two clear bars but no nr. Nuclear bars can also exist in the absence of a clear primary bar, as evidenced by cases such as NGC 4553 (BC) and NGC 7702 (Buta 1991b). There can be little doubt that nuclear bars are related to an ILR just as are nuclear rings (see, e.g., Kormendy 1982; Pfenniger & Norman 1990). Whether either or both features develop in any given galaxy may depend on the strength of the primary bar, the velocity dispersion in the central regions, the central density, the amount of gas transported to the center over time, the effectiveness of dissipation, and the present gas content.

It is worth considering some of the properties of these features because they have been the subject of a few recent theoretical investigations. We are particularly interested in those galaxies which are double barred, i.e., which have both a nuclear bar and a normal primary bar. In Table 5 we compile values of the relative (primary bar, nuclear bar) position angle, θ, for 13 double-barred galaxies. In addition, we also give an estimate of the disk axis ratio, q_d, in order to gauge inclinations. These axis ratios are taken mainly from the SGC, which is based on the deep SRC-J southern sky survey. For some of these galaxies, SGC axis ratios are better indicators of inclination than log R_{25} in RC3, owing to the low surface brightnesses of the outer rings. For 10 of these galaxies, θ is based on ellipse fits to isophotes on I-band CCD images from our library (source "CCD" in Table 5). For NGC 1291 and 1317, we list published values of θ, while for NGC 1097, we have deduced an approximate value of θ from a K-band image illustrated by Forbes *et al.* (1992) and the image of the galaxy on an ESO-R sky survey chart. The significance of the sign of θ is illustrated in Fig. 5. We have assumed trailing spiral arms to assign a sense to each nuclear bar as being either trailing or leading. A leading nuclear bar is tipped ahead of the primary bar while a trailing nuclear bar is tipped behind. The sense is affected by inclination, but the disk axis ratio, q_d, given in Table 5 indicates that at least 7 of the 13 objects may have inclinations less than about 30°. In these cases, θ must be close to the true value. Of the seven objects with $q_d > 0.85$, four (NGC 1291, 1433, 1543, and 3081) have leading nuclear bars and two (NGC 5850 and 6782) have trailing

TABLE 5. Relative position angles of nuclear and primary bars.[a]

Name	θ	q_d	Source of θ
NGC 1097	−85°:	0.76	Forbes et al. 1992, ESO-R
NGC 1291	+30°	0.89	de Vaucouleurs 1975
NGC 1317	±90°	0.87	Schweizer 1980
NGC 1326	+60°	0.79	CCD
NGC 1433	+63°	0.89	CCD, Buta 1986b
NGC 1543	+69°	0.93	CCD
NGC 3081	+50°	0.91	CCD (Buta 1990)
NGC 3358	+27°	0.76	CCD
NGC 5728	−57°	0.78	CCD
NGC 5850	−67°	0.87	CCD
NGC 6782	−29°	0.89	CCD
NGC 7098	−19°	0.76	CCD
ESO 508−78	−71°:	0.81	CCD

Notes to TABLE 5

[a] q_d = axis ratio of outer disk from SGC; for NGC 5850 and ESO 508−78, this ratio is taken from RC3

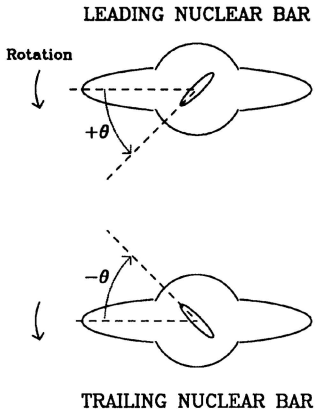

FIG. 5. Schematic which defines the sign of the position angle difference between a primary and a nuclear bar. Rotation direction is deduced by assuming trailing spiral arms.

nuclear bars. The remaining case, NGC 1317, has a 90° alignment.

The *n*-body simulation of Simkin *et al.* (1980) shows that the nuclear oval which develops near an ILR begins as a nuclear ring with a leading sense. It is not clear from such a model whether a trailing nuclear bar or oval could develop. On the other hand, Pfenniger and Norman (1990) point out that if the nuclear bar develops as a result of its own self-gravity, it need not have the same pattern speed as the primary bar. The existence of both leading and trailing nuclear bars could support this idea. Pfenniger and Norman suggest that a favorable situation is for the corotation radius of the nuclear bar to lie near the ILR of the primary bar.

4. CONCLUSIONS

The number of known nuclear rings is still small, but it is likely that they are more common than is generally recognized. Obvious selection effects owing to the location of the rings in the bright central regions of galaxies and their small relative sizes certainly work against their detection on overexposed or small-scale images. The ease with which they are seen in color index maps makes these maps seem like an ideal method with which other nuclear rings may be discovered. A sample focused on early to intermediate Hubble-type galaxies with outer rings and pseudorings provided a 50% return on nuclear ringed or blue nucleus galaxies to BC, and thus such galaxies provide a useful search strategy. The correlation between the presence of distinct, straight dust lanes along the bar and the presence of a nuclear ring suggests another search strategy, because sometimes the dust lanes can be seen on the SRC-J sky survey even when a nuclear ring may not be detectable. Nuclear rings certainly prefer but are not exclusively found in SB galaxies (Sersic & Pastoriza 1967).

We have shown that the spectacular nuclear ring in the southern peculiar galaxy ESO 565−11, highlighted by BC, is the largest clear-cut example in a strong-barred galaxy. The average diameter of nuclear rings is ≈ 1.1 kpc, but the feature in ESO 565−11 has a diameter of nearly 4 kpc. This galaxy demonstrates that normal nuclear rings can achieve sizes that, in more weakly barred galaxies, might cause them to be confused with inner rings. Galaxies like NGC 1302 are in this category and have suspected nuclear rings of a comparable size to that in ESO 565−11.

We have also shown that the large spread in the relative sizes of nuclear rings compared to outer rings can be explained by differences in the rates of rise to maximum and pattern speeds among galaxies with mostly rising rotation curves (as opposed to completely flat rotation curves or rotation curves which fall rapidly outside the nucleus). This is not surprising because an ILR generally would fall in the part of the rotation curve where galaxies differ the most, owing to differences in the mass of the core and the central density. Ring ratios therefore support the interpretation of nuclear rings in terms of the ILR.

Nuclear bars are occasionally associated with nuclear rings. We have shown that these small bars can be of the leading or the trailing sense with respect to the primary bar.

The nuclear ring in NGC 1819 was brought to our attention by E. Davoust. We thank him for allowing us to add this galaxy to our tables. We also thank G. Purcell, F. Bresolin, and L. V. Jones for help with the CCD observations during various observing runs, and an anonymous referee for several helpful comments. This work was supported in part by NSF Grant No. AST 9014137 and NSF EPSCoR Grant No. RII 8996152 to the University of Alabama.

REFERENCES

Arsenault, R., Boulesteix, J., Georgelin, Y., & Roy, J.-R. 1988, A&A, 200, 29
Athanassoula, E. 1992, MNRAS, 259, 345
Athanassoula, E., Bosma, A., Créze, M., & Schwarz, M. P. 1982, A&A, 107, 101
Benedict, G. F. 1980, AJ, 85, 513
Benedict, G. F., Higdon, J. L., Tollestrup, E. V., Hahn, J. M., & Harvey, P. M. 1992, AJ, 103, 757
Benedict, G. F., van Citters, G. W., McGraw, J. T., & Rybski, P. M. 1977, BAAS, 9, 629
Burbidge, E. M., & Burbidge, G. R. 1960, ApJ, 132, 30
Buta, R. 1984, Ph.D. thesis, University of Texas at Austin
Buta, R. 1986a, ApJS, 61, 609
Buta, R. 1986b, ApJS, 61, 631
Buta, R. 1987, ApJS, 64, 383
Buta, R. 1988, ApJS, 66, 633
Buta, R. 1990, ApJ, 351, 62
Buta, R. 1991a, in Dynamics of Galaxies and Their Molecular Clouds Distribution, IAU Symposium No. 146, edited by F. Combes and F. Casoli (Kluwer, Dordrecht), p. 251
Buta, R. 1991b, ApJ, 370, 130
Buta, R., & Crocker, D. A. 1991, AJ, 102, 1715
Buta, R., & Crocker, D. A. 1992, AJ, 103, 1804
Combes, F., & Gerin, M. 1985, A&A, 150, 327
Contopoulos, G., & Grosbol, P. 1989, ARA&A, 1, 261
Corwin, H. G. 1983, private communication
Corwin, H. G., de Vaucouleurs, A., & de Vaucouleurs, G. 1985, Southern Galaxy Catalogue (University of Texas Monographs in Astronomy No. 4, Austin) (SGC)
Crocker, D. A., & Buta, R. 1993, in preparation
Crocker, D. A., Muzerolle, J., & Buta, R. 1993, in preparation
de Vaucouleurs, G. 1959, Handbuch der Physik, 53, 275
de Vaucouleurs, G. 1975, ApJS, 29, 193
de Vaucouleurs, G. 1979, AJ, 84, 1270
de Vaucouleurs, G. 1982, The Cosmic Distance Scale and the Hubble Constant (The Australian National University, Canberra)
de Vaucouleurs, G., & Buta, R. 1980, AJ, 85, 637
de Vaucouleurs, G., de Vaucouleurs, A., Corwin, H., Buta, R., Paturel, G., & Fouqué, P. 1991, Third Reference Catalogue of Bright Galaxies, (Springer, New York) (RC3)
de Vaucouleurs, G., & Peters, W. L. 1981, ApJ, 248, 395
de Vaucouleurs, G., Peters, W. L., Bottinelli, L., Gouguenheim, L., & Paturel, G. 1981, ApJ, 248, 408
Devereux, N. A., Kenney, J. D. P., & Young, J. S. 1992, AJ, 103, 784

Duval, M. F., & Athanassoula, E. 1983, A&A, 121, 297
Elmegreen, B. G., & Elmegreen, D. M. 1990, ApJ, 355, 52
Forbes, D. A., Ward, M. J., DePoy, D. L., Boisson, C., & Smith, M. S. 1992, MNRAS, 254, 509
García-Barreto, J. A., Dettmar, R. J., Combes, F., Gerin, M., Magri, C. & Koribalski, B. 1991a, RM&A, 22, 197
García-Barreto, J. A., Downes, D., Combes, F., Gerin, M., Magri, C., Carrasco, L., & Cruz-Gonzalez, I. 1991b, A&A, 244, 257
Gerin, M., Nakai, N., & Combes, F. 1988, A&A, 203, 44
Hawarden, T. G., Mountain, C. M., Leggett, S. K., & Puxley, P. J. 1986, MNRAS, 221, 41P
Hummel, E., van der Hulst, J. M., & Keel, W. C. 1987, A&A, 172, 32
Jarvis, B. J., Dubath, P., Martinet, L., & Bacon, R. 1988, A&AS, 74, 513
Kormendy, J. 1979, ApJ, 227, 714
Kormendy, J. 1982, ApJ, 257, 75
Lauberts, A., & Valentijn, E. 1989, The Surface Photometry Catalogue of the ESO-Uppsala Galaxies (European Southern Observatory, Munich)
Lindblad, P. O., & Jorsater, S. 1981, A&A, 97, 56
Meaburn, J., Terrett, D. L., Theokas, A., & Walsh, J. R. 1981, MNRAS, 195, 39
Morgan, W. W. 1958, PASP, 70, 364
Osmer, P. S., Smith, M. G., & Weedman, D. W. 1974, ApJ, 192, 279
Pedreros, M., & Madore, B. 1981, ApJS, 45, 541
Peterson, C. J., & Huntley, J. M. 1980, ApJ, 242, 913
Pfenniger, D., & Norman, C. A. 1990, ApJ, 363, 391
Pierce, M. J. 1986, AJ, 92, 285
Pogge, R. W. 1989, ApJS, 71, 433
Roberts, W. W., Huntley, J. M., & van Albada, G. D. 1979, ApJ, 233, 67
Rubin, V. C. 1980, ApJ, 238, 808
Rubin, V. C., Ford, W. K., & Peterson, C. J. 1975, ApJ, 199, 39
Sandage, A. 1961, The Hubble Atlas of Galaxies (Carnegie Institution of Washington Publ. No. 618)
Sandage, A., & Bedke, J. 1988, Atlas of Galaxies Useful for the Cosmological Distance Scale (NASA Publication SP-496)
Schommer, R. A., Caldwell, N., Wilson, A. S., Baldwin, J. A., Phillips, M. M., Williams, T. B., & Turtle, A. J. 1988, ApJ, 324, 154
Schwarz, M. P. 1979, Ph.D. thesis, Australian National University
Schwarz, M. P. 1981, ApJ, 247, 77
Schweizer, F. 1980, ApJ, 237, 303
Scoville, N. Z., Matthews, K., Carico, D. P., & Sanders, D. B. 1988, ApJ, 327, L61
Sérsic, J. L. 1958, Observatory, 78, 125
Sérsic, J. L., & Pastoriza, M. 1965, PASP, 77, 287
Sérsic, J. L., & Pastoriza, M. 1967, PASP, 79, 152
Simkin, S., Su, M. J., & Schwarz, M. P. 1980, ApJ, 237, 404
Telesco, C. M., & Decher, R. 1988, ApJ, 334, 573
Teuben, P. J., Sanders, R. H., Atherton, P. D., & van Albada, G. D. 1986, MNRAS, 221, 1
Wilson, A. S., Helfer, T. T., Haniff, C. A., & Ward, M. J. 1991, ApJ, 381, 79
Wray, J. D. 1988, The Color Atlas of Galaxies (Cambridge University Press, Cambridge)